A Direct-Band-Gap Planar BeN_2 Monolayer with High Mobility and Bilayer-Enhanced Photovoltaic Efficiency

Changping Sun,[1, 2, *] Renyu Duan, [2, *] Hongzhe Pan,[1] Zhaoxin Lu[1], Caoping Niu, [2, †] Meiling Xu,[2,‡] and Yinwei Li[2 †]

[1] College of Physics and Electronic Engineering, Linyi University, Linyi 276000, China

[2] Jiangsu Key Laboratory of Extreme Multi-Field Materials Physics,
School of Physics and Electronic Engineering, Jiangsu Normal University, Xuzhou 221116, China

Corresponding authors: cpniu@jsnu.edu.cn and xml@calypso.cn

Computational details of the CALYPSO method

Crystal structure searches of Be_xN_y ($1 \leq x, y \leq 4$) monolayers were conducted with a maximum of four formula units for each stoichiometry using the Crystal structure AnaLYsis by Particle Swarm Optimization (CALYPSO) method. In the first generation, a population of structures corresponding to certain space group symmetries was randomly generated. Starting from the second generation, 60% of the structures with the lowest enthalpies from the previous generation were selected to generate the next generation using Particle Swarm Optimization (PSO) operators. The remaining 40% of structures in the new generation were generated randomly. A structure finger printing technique of bond characterization matrix is applied to the generated structures, so that identical structures are strictly forbidden. These procedures significantly enhance the diversity of the generated structures, which is critical for improving the efficiency of the global structural search. The search was considered converged when approximately 1000 successive structures had been generated after the lowest-energy structure was found.

Carrier mobility calculations

The carrier mobility of two-dimensional materials based on the deformation potential (DP) theory by Bardeen and Shockley (B-S) formula [1–3]:

$$\mu_{2D} = \frac{e\hbar^3 C_{2D}}{k_B T m^* m_d (E_1)^2}$$

Here, C_{2D}, E_1 and m^* represent the elastic modulus of the longitudinal strain, the deformation potential constant of the VBM for holes or CBM for electrons, and the carrier effective mass in the transport direction, respectively. The C_{2D} is defined as $C_{2D} = 2(E - E_0)/S_0(\Delta l/l_0)^2$, where E, E_0, S_0, l_0 represent the total energy for the compressed/dilated structure, the total energy at equilibrium, the equilibrium lattice area, the equilibrium lattice constant in the transport direction and the deformation of l_0, respectively. The E_1 equals to $\Delta E/(\Delta l/l_0)$, in which E, l, and Δl are donated as the energy change of CBM or VBM under compression or tensile strain, the lattice constants in the transport direction, and the deformation of l_0. m^* is the effective mass in transport direction, and m_d is determined by $m_d = \sqrt{m_x^* m_y^*}$ (m_x^* is perpendicular to m_y^*). The temperature T is set to be 300 K, and k_B is Boltzmann constant.

Absorption spectra calculations

The linear optical properties of semiconductors can be obtained from the frequency-dependent complex dielectric function:

$$\varepsilon(\omega) = \varepsilon_1(\omega) + i\varepsilon_2(\omega)$$

where $\varepsilon_1(\omega)$ and $\varepsilon_2(\omega)$ are the real and imaginary parts of the dielectric function, and ω is the photon frequency. The relevant parameters such as the absorption $\alpha(\omega)$ can be calculated from the real $\varepsilon_1(\omega)$ and the imaginary $\varepsilon_2(\omega)$ parts [4]:

$$\alpha(\omega) = \frac{\sqrt{2}\omega}{c}\left(\sqrt{\varepsilon_1^2 + \varepsilon_2^2} - \varepsilon_1\right)^{\frac{1}{2}}.$$

Polar diagrams for Young's modulus and Poisson's ratio

Using the calculated elastic constants, the Young modulus and Poisson ratio along an arbitrary direction θ (θ is the angle relative to the x direction) are also obtained as [5]

$$E(\theta) = \frac{C_{11}C_{12} - C_{12}^2}{C_{11}s^4 + C_{22}c^4 + (\frac{C_{11}C_{12} - C_{12}^2}{C_{44}} - 2C_{12})c^2s^2}$$

$$v(\theta) = -\frac{(C_{11} + C_{22} - \frac{C_{11}C_{12} - C_{12}^2}{C_{44}})c^2s^2 - C_{12}(c^4 + s^4)}{C_{11}s^4 + C_{22}c^4 + (\frac{C_{11}C_{12} - C_{12}^2}{C_{44}} - 2C_{12})c^2s^2}$$

where $c = \cos\theta$ and $s = \sin\theta$.

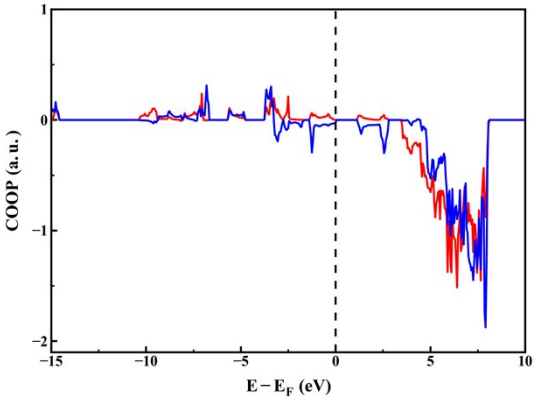

Figure S1. The crystal orbital overlap population (COOP) curves for the shortest Be-N and N-N bonds in the 567-BeN_2 monolayer. Positive and negative values indicate bonding and antibonding states, respectively.

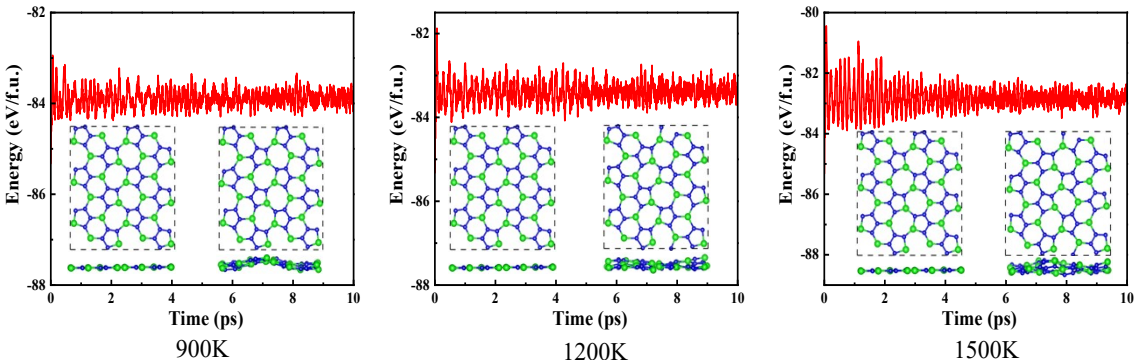

Figure S2. Evolution of energies during AIMD simulations at 900K, 1200 K, and 1500 K of the 567-BeN_2 monolayer. The insets feature structural snapshots captured at the beginning and end of the 10 ps simulation period.

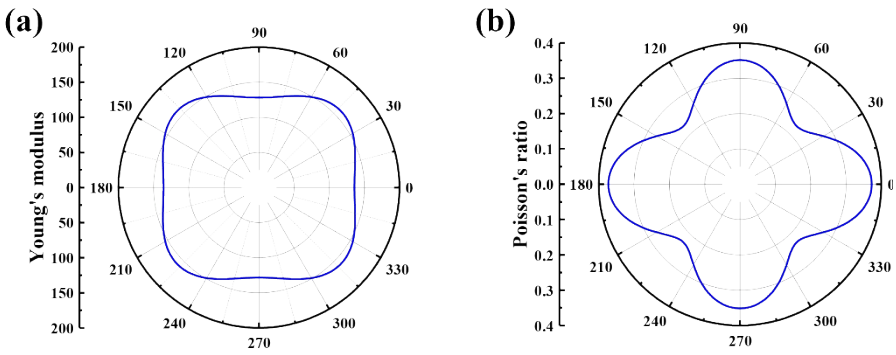

Figure S3. (a) Polar diagrams for Young's modulus (E, Nm^{-1}) and (b) Poisson's ratio (Pr) of the 567-BeN_2 monolayer.

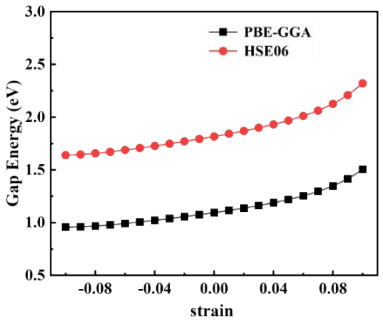

Figure S4. Band gap variation of the 567-BeN_2 monolayer under biaxial strain.

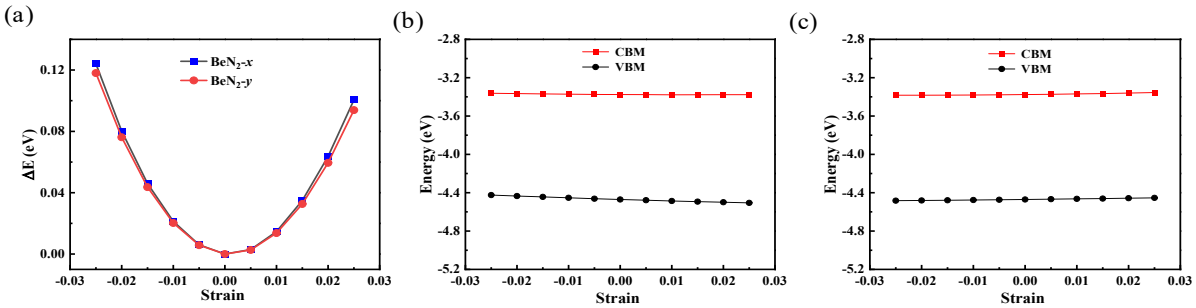

Figure S5. (a) Total energy differences of 567-BeN2 under uniaxial strain from -3% to 3% applied along the x and y directions. (b, c) Strain-induced shifts of the CBM and VBM of monolayer 567-BeN_2 relative to the vacuum level as functions of tensile and compressive lattice deformation along the x and y directions.

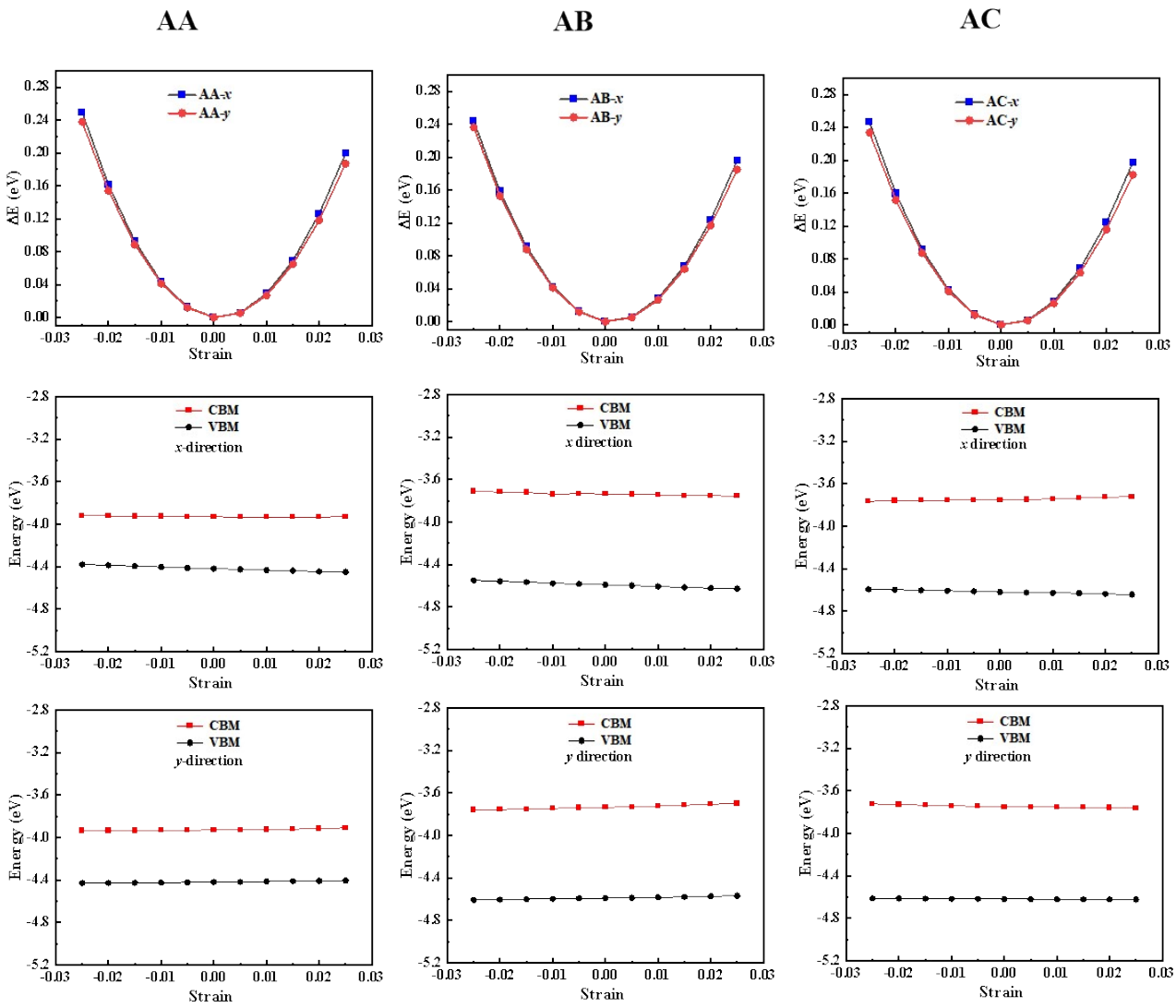

Figure S6. Total energy differences of bilayer 567-BeN_2 under uniaxial strain from -3% to 3% applied along the *x* and *y* directions. Strain-induced shifts of the CBM and VBM of bilayer 567-BeN_2 relative to the vacuum level as functions of tensile and compressive lattice deformation along the *x* and *y* directions.

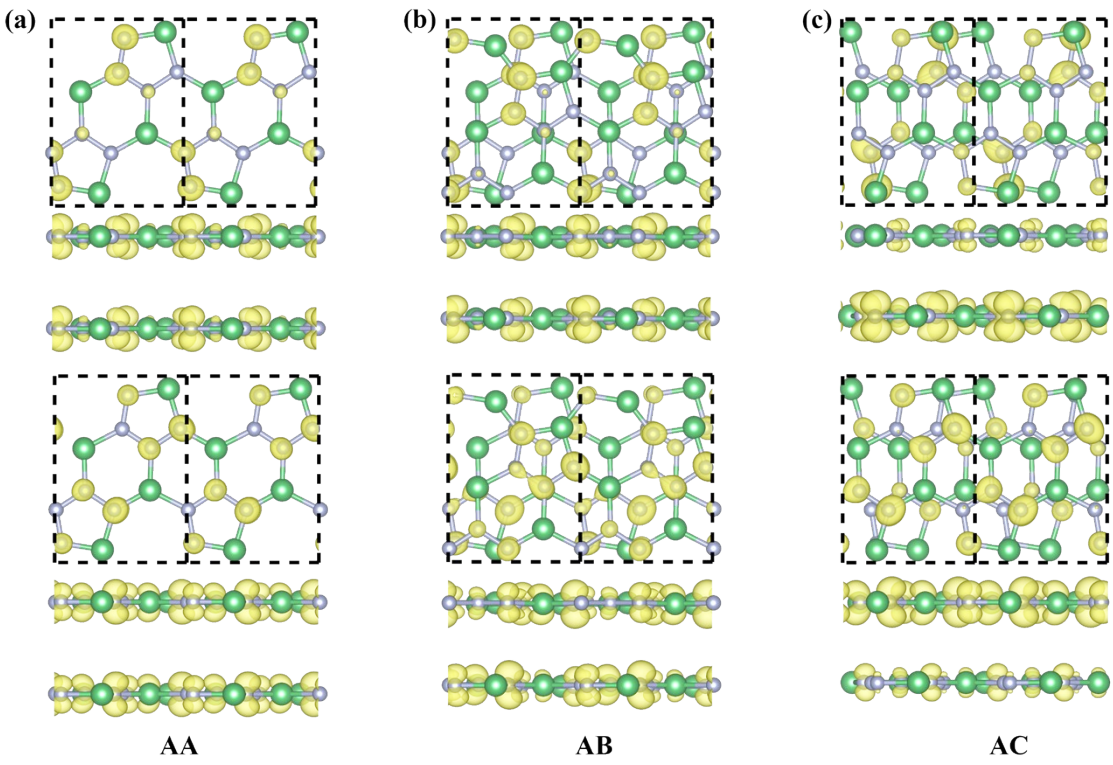

Figure S7. Partial charge density distributions at the conduction-band minimum (CBM) (top panel) and valence-band maximum (VBM) (bottom panel), with an isovalue of 0.007 e/bohr^3 for 567-BeN_2 with (a) AA, (b) AB, and (c) AC stacking configurations.

Table S1. The energy differences among AA-, AB-, and AC- stacking were calculated by the nonlocal optB86b-vdW density functional and DFT-D3 method.

Methods	**Energy (eV/atom)**		
	E_{AA}	E_{AB}	E_{AC}
optB86b	0.011	0.002	0
DFT-D3	0.010	0.002	0

Table S2. The calculated carrier effective masses (m*, m_0), deformation potential constants (E_1, eV), elastic moduli (C, J m^{-2}), and carrier mobilities (μ, 10^3 cm^2 V^{-1} s^{-1}) along the *x* and *y* directions for bilayer 567-BeN_2 with different stacking configurations.

Compounds	**Carrier**	$\mathbf{m^*_x}$	$\mathbf{m^*_y}$	$\mathbf{E_{1x}}$	$\mathbf{E_{1y}}$	$\mathbf{C_{2Dx}}$	$\mathbf{C_{2Dy}}$	$\boldsymbol{\mu_x}$	$\boldsymbol{\mu_y}$
AA	Electron	0.71	0.55	0.24	0.47	359.05	339.79	308.99	96.38
	Hole	0.77	0.93	1.42	0.51	359.05	339.79	5.86	36.17
AB	Electron	0.96	0.62	0.89	1.16	352.08	336.81	12.93	11.23
	Hole	1.11	0.73	1.57	0.78	352.08	336.81	3.06	18.16
AC	Electron	0.70	0.69	0.78	0.04	355.27	333.03	23.98	28.86
	Hole	0.66	1.58	0.98	0.54	355.27	333.03	12.35	97.61

Table S3. The calculated elastic constants (C_{ij}, N/m), Young's modulus (E_Y, N/m) and Poisson's ratio (P_r) of 567-BeN_2 with AA, AB, and AC stacking configurations.

Stacking configurations	C_{11}	C_{22}	C_{12}	C_{66}	E_{Yx}	E_{Yy}	P_{rx}	P_{ry}
AA	312.88	296.10	111.06	129.21	273.46	254.44	0.375	0.355
AB	306.49	293.19	108.14	127.76	268.33	253.31	0.369	0.353
AC	312.88	296.10	111.06	129.21	273.46	254.44	0.380	0.356

POSCAR file for 567-BeN_2

1:P2_1(4)

1.00000000000000

7.2613375730364007 0.0000000000000000 0.0000000000000000

0.0000000000000000 5.1314224559102914 0.0000000000000000

0.0000000000000000 0.0000000000000000 30.0000000000000000

Be N

4 8

Direct

0.6112267048744116 0.7781903829390160 0.5000000000000000

0.9307494116574730 0.1381407107257360 0.5000000000000000

0.0692505883425270 0.6381407107257360 0.5000000000000000

0.3887732951255884 0.2781903829390160 0.5000000000000000

0.8961996270314643 0.4469053463607082 0.5000000000000000

0.7169416553453587 0.0490408121131694 0.5000000000000000

0.2830583446546413 0.5490408121131694 0.5000000000000000

0.1038003729685357 0.9469053463607082 0.5000000000000000

0.7163014311933225 0.4885294841035019 0.5000000000000000

0.6157649864629988 0.2688832637578571 0.5000000000000000

0.3842350135370012 0.7688832637578571 0.5000000000000000

0.2836985688066775 0.9885294841035019 0.5000000000000000

References

[1] Bruzzone, Samantha, and Gianluca Fiori. "Ab-initio simulations of deformation potentials and electron mobility in chemically modified graphene and two-dimensional hexagonal boron-nitride." *Applied Physics Letters* 99.22 (2011).

[2] Fiori, Gianluca, and Giuseppe Iannaccone. "Multiscale modeling for graphene-based nanoscale transistors." *Proceedings of the IEEE* 101.7 (2013): 1653-1669.

[3] Takagi, Shin-ichi, et al. "On the universality of inversion layer mobility in Si MOSFET's: Part I-effects of substrate impurity concentration." *IEEE Transactions on Electron Devices* 41.12 (1994): 2357-2362.

[4] Fox, Mark. *Optical properties of solids*. Vol. 3. Oxford university press, 2010.

[5] Zhang, Chenxi, Jun Lou, and Jizhou Song. "A cohesive law for interfaces in graphene/hexagonal boron nitride heterostructure." *Journal of Applied Physics* 115.14 (2014).